Civil Engineering Dimension
https://ced.petra.ac.id

Experimental Investigation on Seismic Performance of Precast Column-Foundation Connection using Combined Anchor and Pocket System

Propika, J.[1,2*] , Pudjisuryadi, P.[1], and Chandra, J.[1]
[1] Department of Civil Engineering, Petra Christian University, Surabaya, INDONESIA
[2] Department of Civil Engineering, Adhi Tama Institute of Technology, Surabaya, INDONESIA

DOI: https://doi.org/10.9744/ced.28.1.69-82

Article Info:
Submitted: June 21, 2025
Reviewed: July 12, 2025
Accepted: Dec 09, 2025

Keywords:
precast concrete,
column–foundation connection,
pocket connection,
anchored reinforcement,
seismic performance,
cyclic loading,
energy dissipation.

Corresponding Author:
Propika, J.
Department of Civil Engineering,
Adhi Tama Institute of Technology,
Surabaya, INDONESIA
Email: jakapropika@itats.ac.id

Abstract

Connections between precast concrete elements play a crucial role in ensuring structural integrity and facilitating effective force transfer. Among various connection types, the column–foundation connection is the most critical component, as it is designed to resist the combined effects of axial load, bending moment, and shear force. In this study, the pocket connection was modified with anchored reinforcement (BPC) to improve seismic performance. An experimental program was conducted on three specimens: a monolithic cast-in-place connection (MC) as the control, a conventional pocket connection (PC), and the modified pocket connection (BPC). Each specimen was subjected to combined axial and cyclic loading to evaluate the seismic performance of the column–foundation connection. The results showed that the MC specimen demonstrated the best performance, while the PC specimen, although meeting the ACI 374.1-05 acceptance criteria, failed to achieve the required probable moment capacity. The BPC specimen demonstrated improvement in seismic performance compared to the PC and was considered suitable for use in precast structural systems designed for seismic area.

INTRODUCTION

The use of precast concrete structures has become increasingly popular due to several advantages over cast-in-place concrete, including improved quality control, shorter construction time, ease of replacing damaged elements, reduced construction waste, and overall cost efficiency [1–9]. However, numerous precast structures have suffered significant damage or failure during major earthquakes such as the 1994 Northridge, 1999 Marmara, and 2012 Emilia events [10]. These failures were mainly attributed to inadequate connection detailing, as connections play a vital role in force transfer and strongly influence the global performance and reliability of the structure [11–15]. Among various connection types, the column–foundation connection is considered the most critical since it must resist the combined effects of axial load, bending moment, and shear force [16,17]. In seismic-resistant structural systems, particularly Special Moment Frames (SMFs), precast connections must ensure adequate deformation capacity and energy dissipation under cyclic loading [18–20].

Column–foundation connections can generally be classified into three main types: base plate connections, pocket foundation connections, and grouted sleeve connections. Among these, the pocket foundation connection has demonstrated favorable performance in terms of ductility and energy dissipation [8,21]. This system is also preferred

Note : Discussion is expected before July, 1st 2026, and will be published in the "Civil Engineering Dimension", volume 28, number 2, September 2026.
ISSN : 1410-9530 print / 1979-570X online
Published by : **Petra Christian University**

for its ease of assembly and tolerance to construction inaccuracies [22]. In contrast, grouted sleeve connections require tight dimensional tolerances, high precision, and relatively expensive grout materials [23]. For these reasons, socket-type pocket connections are often regarded as the most practical and reliable alternative, and several standards such as FIB Bulletin 43, EN 1992-1-1, and the PCI Design Handbook (7th Edition) provide detailed design guidance [24]. The pocket system transfers forces by embedding the precast column base into a foundation pocket filled with grout, where performance is influenced by embedment depth, grout strength, and concrete quality [25–27].

Previous studies have shown that an embedment depth of 1.2D–1.5D can achieve performance comparable to monolithic connections. However, such large embedment depths are often structurally and economically inefficient, as they require thicker foundation blocks to accommodate the column embedment, increasing self-weight and construction cost. Although a deeper embedment enhances strength, it may not represent an optimal design solution. To address this limitation, this study reduces the embedment depth to 0.5D while maintaining sufficient strength and ductility, aiming for a more efficient and practical alternative.

Studies focusing on improving the load-transfer mechanism and ductility of pocket connections under cyclic loading remain limited, as most previous research has primarily examined the effect of embedment depth. To fill this research gap, this study proposes a modified precast column–foundation connection system combining a pocket foundation and anchored reinforcement (BPC) to enhance strength, stiffness, ductility, and energy dissipation capacity. Three specimens were tested: (1) a monolithic cast-in-place connection (MC), (2) a conventional pocket connection (PC) with 0.5D embedment, and (3) a modified pocket–anchor connection (BPC). The experimental results were analyzed to compare structural behavior, assess compliance with the ACI 374.1-05 acceptance criteria, and evaluate the potential of the proposed system for seismic-resistant precast structures. The outcomes of this study are expected to provide practical recommendations for designing efficient, ductile, and earthquake-resistant precast column–foundation connections.

EXPERIMENTAL PROGRAM

Specimens Design

This study experimentally investigated three types of precast column–foundation connections with different configurations: monolithic cast-in-place (MC), pocket connection (PC), and modified pocket–anchor connection (BPC). The MC specimen served as the control, representing a conventional monolithic joint, while PC and BPC represented precast configurations designed to evaluate the effect of connection detailing. All specimens were constructed with identical geometry and reinforcement to ensure that performance variations were solely attributed to the connection type. The main parameters of the specimens are summarized in Table 1.

Table 1. Main Parameters of the Column-foundation Connections

Specimen type	Column Reinforcement		Anchors	Pocket depth (mm)	Column Moment Probable M_{pr} (kNm)	Expected Lateral Force V_e (kN)
	Longitudinal	Stirrups				
MC	8D16	3D10-75	-	-	152	82.16
PC	8D16	3D10-75	-	150	150	81.08
BPC	8D16	3D10-75	4D19	200	139	75.14

The configurations of the three specimens are shown in Figure 1. The MC specimen (Figure 1a) was constructed through continuous cast-in-place concreting in accordance with the Special Moment Frame (SMF) provisions of ACI 318-14. It served as the benchmark to assess the performance of precast alternatives under cyclic lateral loading. The PC specimen (Figure 1b) employed a pocket connection system with smooth interior walls and a shallow embedment depth of 0.5D. This design intentionally deviated from the recommendations of PCI and EN 1992-1-1 ($\geq 1.0D - 1.5D$) to examine the performance and failure mechanism of shallow-embedment connections and to evaluate the efficiency of the grout in transferring loads between precast components. The BPC specimen (Figure 1c) represented the developed configuration, integrating the pocket system with mechanical anchor reinforcement (4D19) embedded into the foundation. This hybrid mechanism was designed to enhance load transfer efficiency, ductility, and seismic performance. Testing of the BPC specimen focused on assessing the interaction between the pocket and anchor mechanisms under cyclic lateral loading.

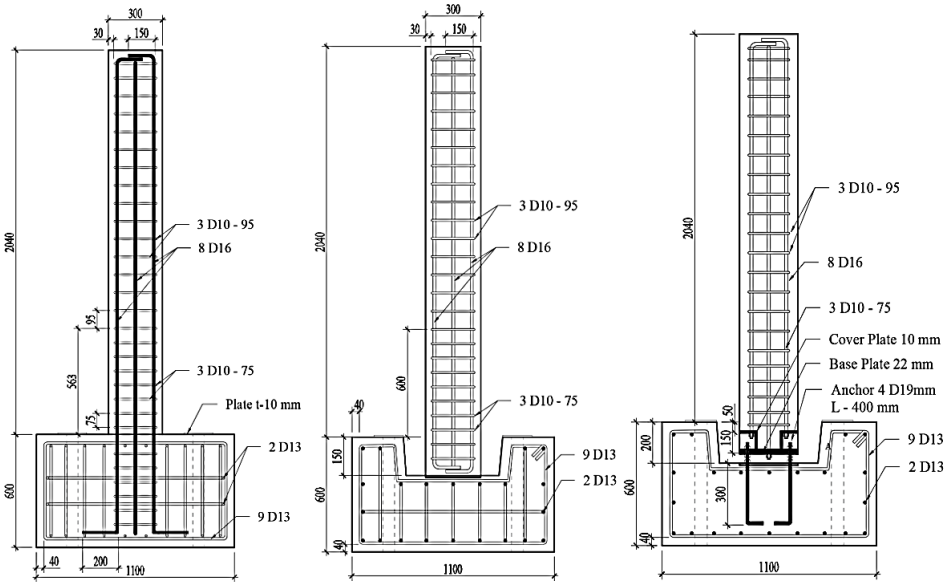

(a) (b) (c)

Figure 1. Details of Specimen Geometry and Reinforcement: (a) MC; (b) PC; (c) BPC

Material Properties

Material tests were conducted to determine the compressive strength of concrete and grout and the tensile properties of reinforcing and anchor steels. Compressive strength tests were performed in accordance with ASTM C39/C39M-21, while tensile tests followed ASTM E8/E8M-09 and ASTM A615/A615M standards. The test results for concrete and grout are summarized in Table 2, the mechanical properties of reinforcing and anchor steels are presented in Table 3.

Table 2. Concrete and Grouting Material Specifications

Specimen Type	Concrete Compressive Strength, f'_c (MPa)	Grouting Strength, f'_{cg} (MPa)
MC	48.53	-
PC	47.74	52.60
BPC	41.34	42.22

Table 3. Reinforcement and Anchor Material Specifications

Rebar Diameter (mm)	Section Area (mm^2)	Tensile Strength		Elongation in 200 mm	Ratio f_u/f_y
		f_y (MPa)	f_u (MPa)	(%)	
D.19	271.26	461.78	621.64	23	1.35
D.16	193.23	478.89	608.22	22.5	1.27
D.13	124.19	466.11	617.31	22	1.32
D.10	73.53	486.04	648.29	18	1.33
Anchor D.19	276.44	473.89	501.79	5.47	1.06

Based on the material test results, most materials satisfied the minimum strength requirements for earthquake-resistant reinforced concrete structures, except for the anchor steel, which exhibited a lower ultimate tensile strength than that specified for seismic-grade applications. However, since the anchor bars were used only in the BPC specimen, the test results will be evaluated with respect to the actual material properties rather than ideal seismic specifications.

Therefore, the performance comparison among the MC, PC, and BPC specimens can still be considered valid and representative of the material conditions used in this study.

Test Set Up, Instrumentations, and Loading Scheme

The instrumentation configuration is illustrated in Figure 2. A total of 14 Linear Variable Differential Transformers (LVDTs) were installed to record the structural response throughout the test. LVDTs 1–2 measured the lateral

displacement at the column tip, LVDTs 3–4 monitored horizontal sliding, LVDTs 5–6 captured shear deformation at the column base, LVDTs 7–8 detected vertical movement of the foundation, and LVDTs 9–14 measured flexural deformation induced by lateral loading. Strain gauges (SGs) were positioned at critical locations expected to experience significant strain. For the MC and PC specimens, SGs were attached to the longitudinal and transverse reinforcement around the plastic hinge region. In the BPC specimen, additional SGs were mounted on the anchor bars to monitor the effectiveness of the connection in transferring forces between the precast column and the foundation.

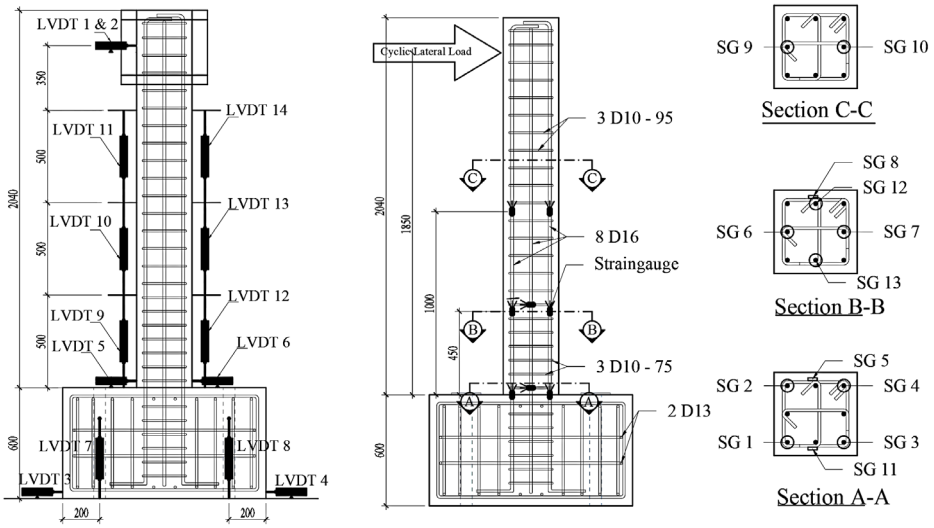

Figure 2. Instrumentation Layout of LVDTs and Strain Gauges during Specimen Testing

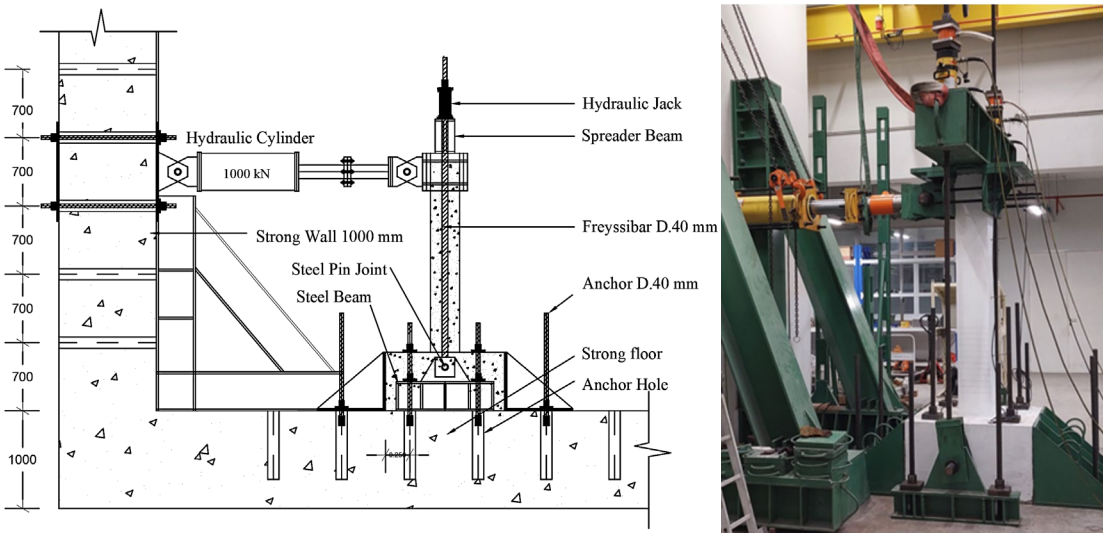

Figure 3. Test Set Up

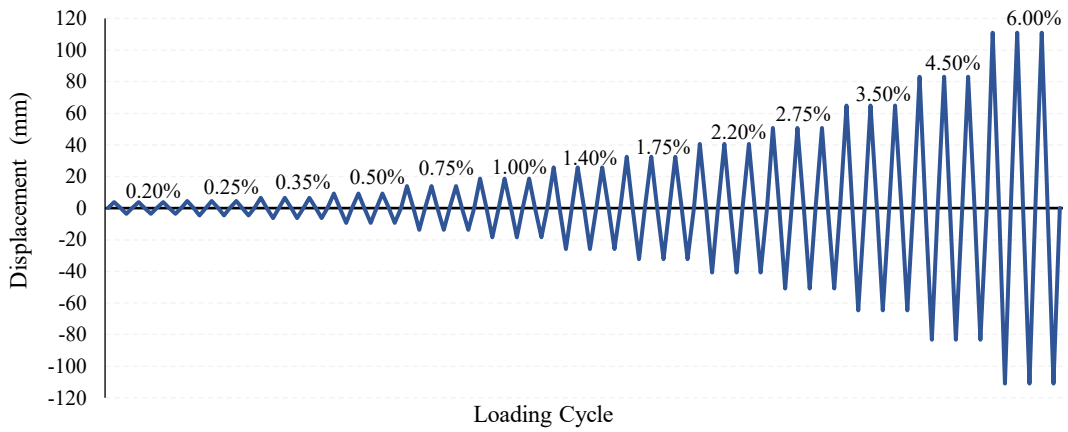

Figure 4. Loading Protocol

The loading configuration is illustrated in Figure 3. All three specimens were subjected to a constant axial load corresponding to 15% of the nominal axial capacity of the column, representing the effect of gravity loads. This axial load was applied and maintained throughout the entire testing process. A cyclic lateral load was applied at the top of the column, at a height of 1850 mm above the foundation, to simulate the seismic loading effects. The loading protocol adopted in this study followed a displacement-controlled cyclic loading procedure, with a maximum target drift ratio of 6 %. The cyclic loading history was developed in accordance with the provisions of ACI 374.1-05 [35], as illustrated in Figure 4.

RESULTS AND DISCUSSION

Failure Mechanism

Figure 5a shows the condition of specimen MC after testing. The first crack appeared at a drift ratio of 0.35% under a lateral load of 36.5 kN, and progressively widened with increasing loading cycles until spalling of the concrete cover occurred at a drift ratio of 2.20% with a maximum load of 88.0 kN, marking the onset of lateral strength degradation. Initial damage was observed in the plastic hinge region, approximately 300–400 mm above the foundation, and extended up to 600 mm by the end of the test. *Strain gauge* readings at Section A–A (Figure 2) indicated first yielding of the longitudinal reinforcement at a drift ratio of 1.40%, while no yielding occurred at Sections B–B and C–C. The transverse reinforcement at Section A–A yielded at a drift ratio of 2.75%.

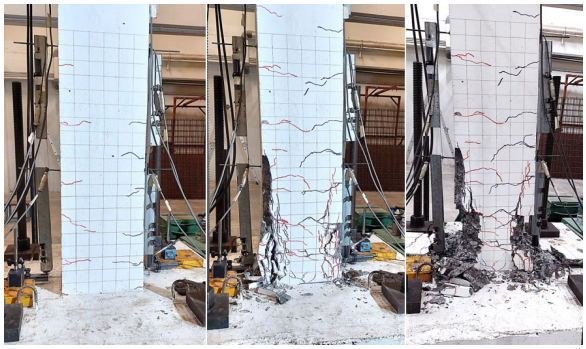

Drift 0.50% Drift 3.50% Drift 6.00%

(a)

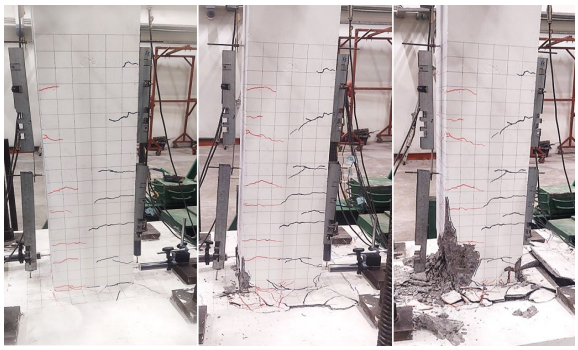

Drift 0.50 % Drift 3.50 % Drift 6.00 %

(b)

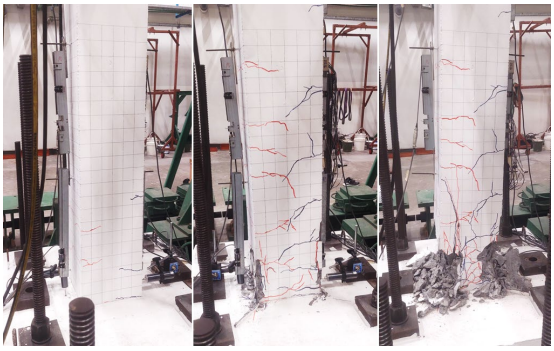

Drift 0.50% Drift 3.50% Drift 6.00%

(c)

Figure 5. Damage Patterns of Precast Column-Foundation Connections: (a) MC; (b) PC; (c) BPC

For specimen PC (Figure 5.b), the first crack in the column occurred at a *drift ratio* of 0.35% under a lateral load of 35.5 kN. The first crack in the grouting pocket appeared at a *drift ratio* of 1.0%, and significant grout damage developed at 2.20% with a load of 56 kN. Surface spalling of the column was observed at a *drift ratio* of 2.75% under a lateral load of 56.5 kN. Visual observations indicated that the failure was governed by the connection system, as evidenced by limited crack propagation in the column beyond a *drift ratio* of 2.20%. *Strain gauge* data confirmed that neither longitudinal nor transverse reinforcement yielded during testing. These results demonstrate that connection failure occurred prior to the column reaching its plastic capacity, and the structural response was therefore classified as a *connection-controlled failure*.

For specimen BPC (Figure 5c), the first crack was observed at a *drift ratio* of 0.35% in the plastic hinge region, approximately 125 mm above the column–foundation interface. As the loading cycles increased, cracks propagated and led to spalling of the concrete cover at a *drift ratio* of 2.75%. Unlike specimen MC, the initial damage in this specimen was concentrated at the base of the column, particularly around the column–foundation connection. LVDT readings confirmed both lateral displacement and rotational movement at the connection zone. Cracking in the grouting material appeared at a *drift ratio* of 0.75%, but showed no significant propagation in subsequent cycles. Overall, the damage was confined to the lower part of the column, indicating a flexural failure mechanism. *Strain gauge* measurements revealed that the 4D19 anchor bars remained elastic, while the 8D16 longitudinal reinforcement yielded at Section A–A, and the transverse reinforcement remained within the elastic range.

In general, the experimental results revealed distinct failure mechanisms among the tested specimens, primarily influenced by their connection configurations. These findings emphasize that connection detailing plays a crucial role in governing the failure mechanism and deformation capacity of precast concrete columns under cyclic loading.

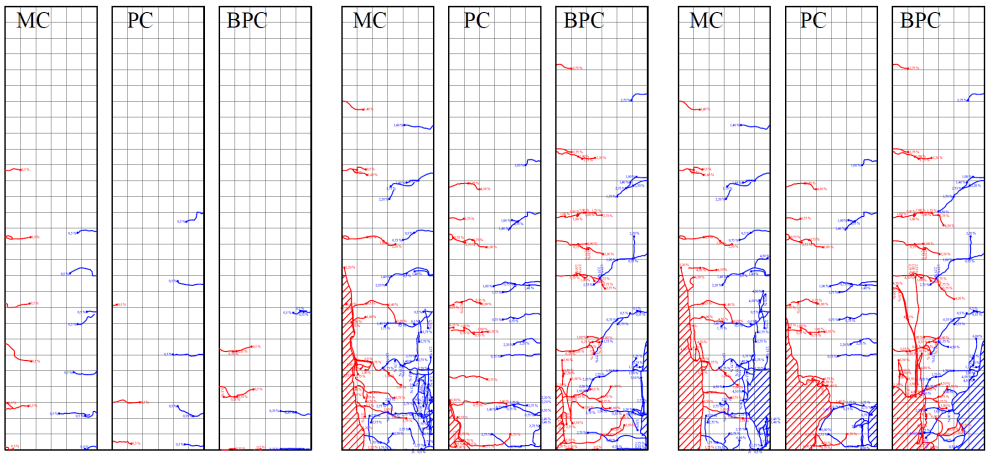

Figure 6. Comparison of the Damage Patterns of Each Specimen

Figure 6 compares the damage patterns of the three column–foundation connection specimens — MC, PC, and BPC — at *drift ratios* of 0.50% (elastic range), 3.50% (minimum drift limit for *Special Moment Frame*, SMF), and 6% (final testing stage). The MC specimen exhibited the most severe damage, characterized by extensive cracking and spalling of the concrete cover beyond a *drift ratio* of 2.20%. The monolithic stiffness of the connection induced high stress concentrations in the plastic hinge zone, accelerating crack propagation and leading to a gradual reduction in lateral strength. Nevertheless, MC achieved the highest lateral load capacity among all specimens. In contrast, the PC specimen showed the least column damage. At a *drift ratio* of 2.20%, crushing of the grout material inside the pocket reduced the joint's moment transfer capacity. This triggered rotation at the column–foundation interface, shifting deformation from the column element to the joint region and decreasing both stiffness and moment capacity. Meanwhile, the BPC specimen demonstrated more controlled damage than MC. The combination of a smooth-walled pocket (0.5D depth) and 4D19 anchor bars enabled an effective rotational mechanism at the joint. Deformation of the steel cover plate and localized grout cracking provided additional flexibility, promoting moment redistribution and enhancing energy dissipation. *Strain gauge* data revealed anchor bar strains approaching the yield limit, indicating the dominant contribution of the anchorage system in transferring lateral loads. As a result, BPC achieved a lateral load capacity comparable to MC, but with a less severe damage pattern.

Overall, the connection configuration significantly influenced the structural response under cyclic lateral loading. The MC connection provided high stiffness and strength but was prone to severe damage. The BPC connection

exhibited balanced performance, combining sufficient capacity with improved deformability through joint rotation and anchor action. In contrast, the PC connection effectively protected the column element but suffered a marked reduction in lateral capacity due to premature grout failure, preventing the development of the probable moment capacity of the column.

Cyclic Response

This section analyzes and compares the cyclic response behavior of the three column–foundation connections(MC, PC, and BPC)based on the hysteretic and backbone curves shown in Figure 7. The results are further evaluated against the acceptance criteria of ACI 374.1-05, focusing on the nominal and maximum strength capacities summarized in Tables 4 and *5*.

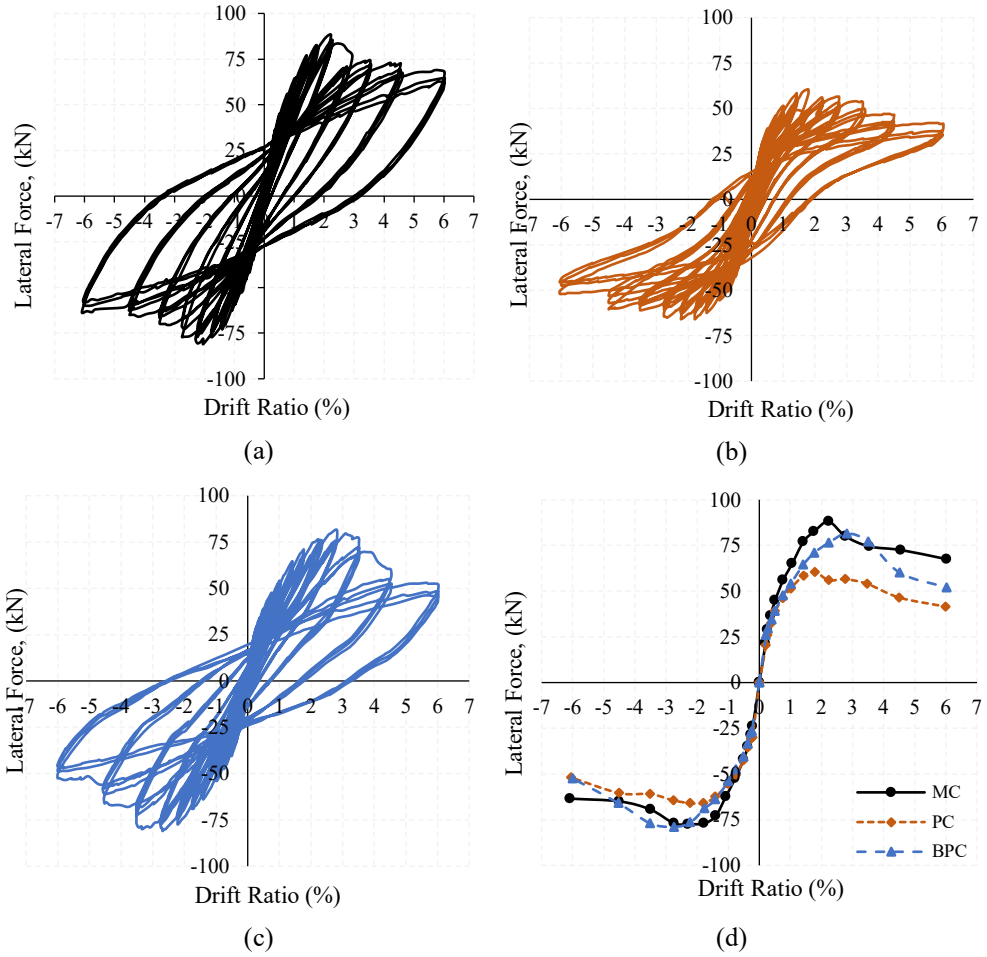

Figure 7. Hysteretic Response of the Test Specimens: (a) MC; (b) PC; (c) BPC; and (d) Backbone Curve

Table 4. Acceptance Criteria for Strength Capacity According to ACI 374.1-05

Specimen	Nominal Momen, M_n $(kN.m)$	Nominal Lateral Force, E_n (kN)	Probable Moment, M_{pr} $(kN.m)$	Probable Lateral force, E_{pr} (kN)	Maximum Moment M_{max} $(kN.m)$	Maximum Lateral force, E_{max} (kN)	Nominal Lateral Drift, Δ_n (%)	Acceptance Criteria
MC	105.9	57.2	151.0	81.6	162.8	88.0	0.85	Satisfied
PC	105.3	56.9	150.0	81.1	122.1	66.0	1.38	Satisfied
BPC-2	102.9	55.7	147.0	79.5	150.7	81.5	1.10	Satisfied

Tabel 5. Maximum Strength Acceptance Criteria

Specimen	Maximum force (kN)		Force at 3.5% (kN)		Ratio $E_{\Delta,3.5\%^+}/E_{max^+}$		Acceptance Criteria
	E_{max^+}	E_{max^-}	$E_{\Delta,3.5\%+}$	$E_{\Delta,3.5\%+}$	Positive (%)	Negative (%)	
MC	88.0	-81.0	69.5	-64.5	78.98	79.63	Satisfied
PC	66.0	-60.5	57.0	-47.0	86.36	77.69	Satisfied
BPC-2	81.5	-81.0	69.0	-68.5	84.66	84.57	Satisfied

Figure 7a presents the hysteresis curve of the MC specimen. The maximum lateral load recorded was 88 kN, corresponding to a maximum moment of 162.8 kNm at a *drift ratio* of 2.20%, which exceeds the probable flexural strength of the column (Mpr = 151 kNm). This indicates that the connection exhibited a higher strength capacity than the column section itself.

The nominal lateral load obtained from the analytical results was 57.23 kN at a *drift ratio* of 0.845%, satisfying the acceptance requirement of ACI 374.1-05 Section 9.1.1, which specifies that each specimen must reach its nominal design strength (En) before exceeding the allowable *story drift* limit of 1.5–2.5% defined in ASCE/SEI 7-10. At a *drift ratio* of 3.5% (third loading cycle), the measured lateral loads were 69.5 kN in the positive direction and 64.5 kN in the negative direction, representing 78.98% and 79.63% of the peak lateral load, respectively. These values fulfill the requirement of ACI 374.1-05 Section 9.1.2.1, which mandates that at the third cycle with a *3.5% drift ratio*, the specimen must maintain at least 75% of its maximum lateral strength (Emax).

Figure 7b presents the hysteresis curve of the PC specimen. The maximum lateral load recorded was 66 kN, corresponding to a maximum moment of 122.1 kNm at a *drift ratio* of 2.20%. This value is lower than the probable moment of the column (Mpr = 150 kNm) but exceeds the nominal analytical moment (Mn = 105.3 kNm), thereby satisfying the strength capacity requirement specified in ACI 374.1-05 Section 9.1.1. At a *drift ratio* of 3.5%, a reduction in lateral strength was observed, however, the residual load remained above 75% of the peak lateral strength (Emax), meeting the acceptance criterion of ACI 374.1-05 Section 9.1.2.1. These results indicate that the PC connection maintained adequate lateral capacity up to the deformation limits required for moment-resisting frame systems.

Figure 7c presents the hysteresis curve of the BPC specimen. The maximum lateral load of 81.5 kN was achieved at a *drift ratio* of 2.75%, corresponding to a maximum moment of 150.78 kNm, which exceeded the probable moment of the column (Mpr = 139 kNm). The nominal lateral load occurred at a *drift ratio* of 1.1%, indicating that the BPC specimen satisfied the minimum drift requirement specified in ASCE/SEI 7-10. A significant reduction in lateral capacity was observed within the *drift ratio* range of 3.5%–4.5%. At a *drift ratio* of 3.5%, the residual capacity remained at 88.34% of the peak load, satisfying the minimum 75% requirement defined in ACI 374.1-05. However, at *drift ratios* of 4.5% and 6%, the capacity decreased to 60.5 kN (74.23%) and 52 kN (63%), respectively. Despite this reduction at higher drifts, the BPC specimen met all acceptance criteria of ACI 374.1-05, including those related to nominal strength capacity and maximum strength degradation limits.

Deformation Contribution

The deformation contribution refers to the portion of total displacement induced by cyclic lateral loading in precast columns. This evaluation, based on LVDT measurements at critical points, assesses the structural performance. Column deformation is mainly governed by flexural and sliding mechanisms, which are the focus of this discussion in line with the observed damage patterns.

As shown in Figure 8, specimens MC, PC, and BPC exhibited flexural deformation as the dominant component of the overall structural deformation mechanism. For specimen MC, flexural deformation contributed more than 70% of the total deformation throughout the drift cycles in both positive and negative directions, while sliding deformation remained relatively small, below 10%. These results indicate that the structural response was primarily governed by flexural behavior, with the deformation mechanism mainly controlled by flexural damage within the column's plastic hinge region. For specimen PC, as shown in Figure 8b, the flexural deformation response under cyclic loading exhibited a significant asymmetry between the positive and negative loading directions. This difference was primarily caused by grout joint damage within the pocket connection, which initiated at a drift ratio of 1.0% and completely deteriorated at 2.2%. The grout degradation altered the deformation pattern on the column face under positive loading, where flexural deformation decreased notably due to dominant base rotation. In contrast, on the negative loading side, the grout remained largely intact, allowing flexural deformation to remain dominant, with an average contribution exceeding 70%, while the shear deformation contribution remained below 5%. For specimen BPC (Figure 8c), flexural deformation was also the dominant component, although with larger fluctuations compared to MC. A significant spike in flexural contribution was observed around a drift ratio of ±1%, exceeding 90%, which likely indicates internal redistribution due to changes in the load-transfer mechanism within the precast connection. Despite this, the average flexural contribution remained within the range of 70–75%, similar to specimen MC. The sliding deformation contribution in specimen BPC also remained low (<10%), but slightly increased at larger drifts (>3%), suggesting potential relative displacement between connection elements under large deformations.

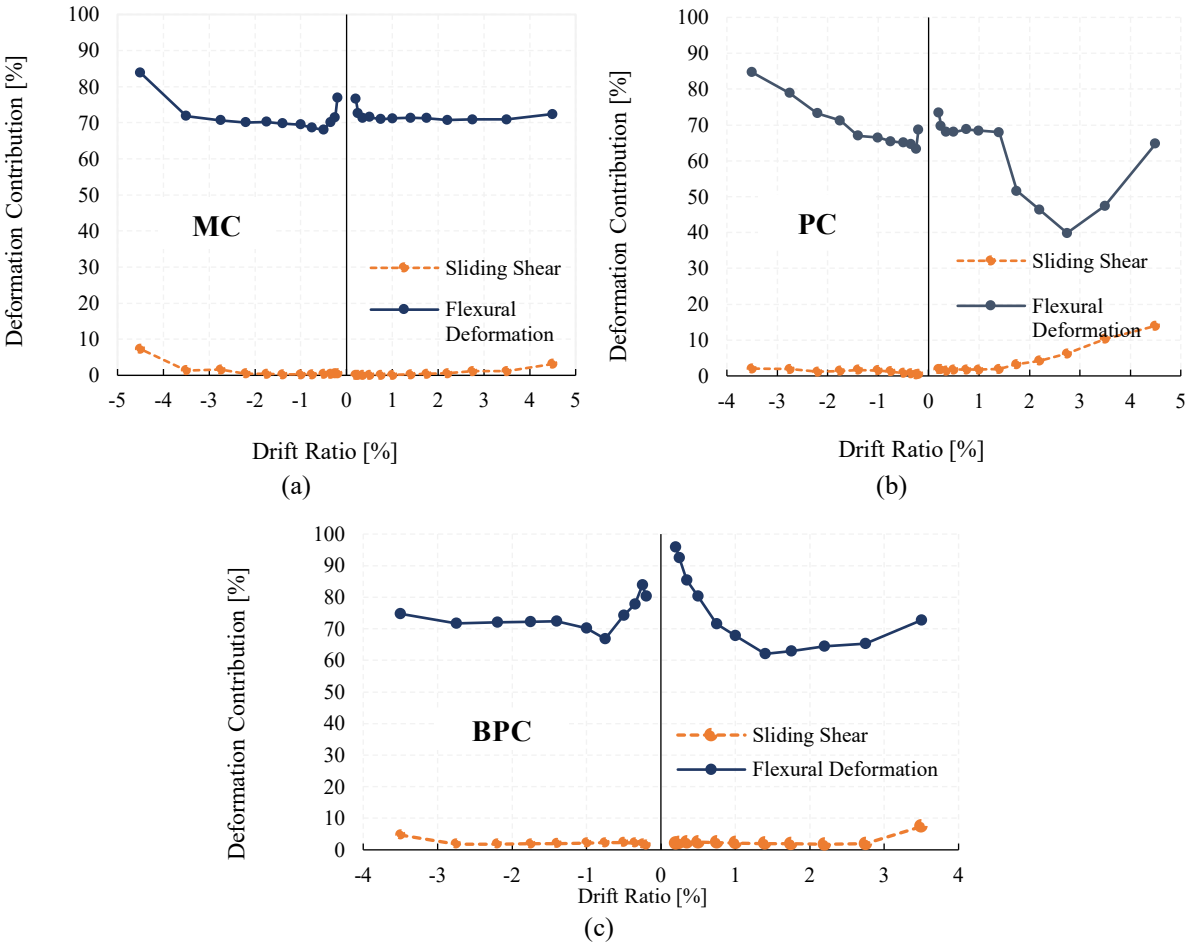

Figure 8. Comparison of Deformation Contribution Curves for Each Specimen: (a) MC; (b) PC; and (c) BPC

Overall, flexural deformation remained the dominant mode across all connection types, with the MC specimen demonstrating the most stable flexural contribution throughout cyclic loading. This highlights the superior structural integrity of the monolithic system in sustaining plastic deformation, whereas the PC and BPC systems exhibited greater variability due to the mechanical complexity of their joints. These findings suggest that monolithic connections provide more reliable deformation performance under cyclic loading, while the BPC system still offers acceptable seismic performance, but requires closer consideration of interaction effects between its components at large deformation levels.

Energy Dissipation

The inelastic performance of a structure is evaluated based on its ability to absorb and dissipate energy induced by lateral seismic loads. A structure with adequate energy dissipation capacity can withstand repeated loading cycles without experiencing brittle failure. According to ACI 374.1-05 (Section 9.1.3), the performance of reinforced concrete elements or connections under cyclic testing is assessed using the Relative Energy Dissipation Ratio (REDR). At the third cycle with a 3.5% drift ratio, the REDR value must be ≥ 0.125 in each loading direction (Figure 9). The REDR is calculated as the ratio of the energy dissipated by the element (area of the hysteresis loop) to the theoretical elastic energy in the same cycle.

Figure 10a illustrates the comparison of cumulative energy dissipation at each cycle for all specimens. The MC specimen exhibited the highest cumulative energy dissipation capacity compared to the PC and BPC specimens. The differences between cycles were relatively small and consistent, indicating ductile and stable behavior. This consistency reflects the structure's ability to withstand repeated deformations without significant strength degradation due to major or sudden damage. Conversely, the PC specimen showed the lowest energy dissipation capacity. Although the variation between cycles was relatively large, the overall decline pattern remained consistent, suggesting that the structure still exhibited stable cyclic behavior. Nevertheless, the overall energy dissipation capacity was relatively low, indicating a less effective energy-dissipating mechanism. For the BPC specimen, the cumulative energy dissipation values were recorded at 22.74 kNm in the first cycle, 19.17 kNm in the second cycle,

and 18.34 kNm in the third cycle. A notable reduction in dissipated energy was observed between cycles, particularly at a drift ratio of 4.5%, indicating uncontrolled damage.

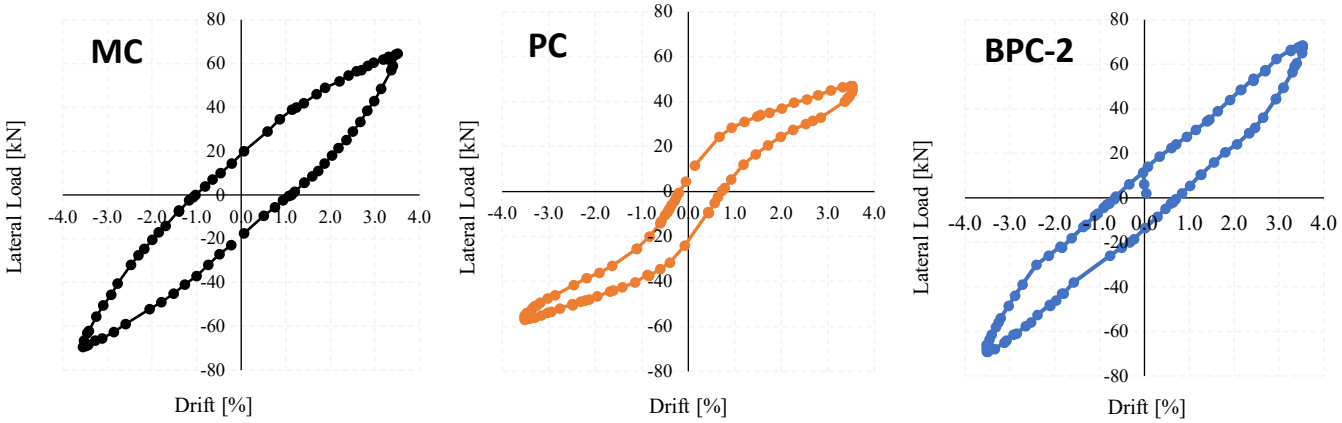

Figure 9. Comparison of the Hysteresis Loop Area at the Third Cycle with 3.5% Drift for Each Specimen

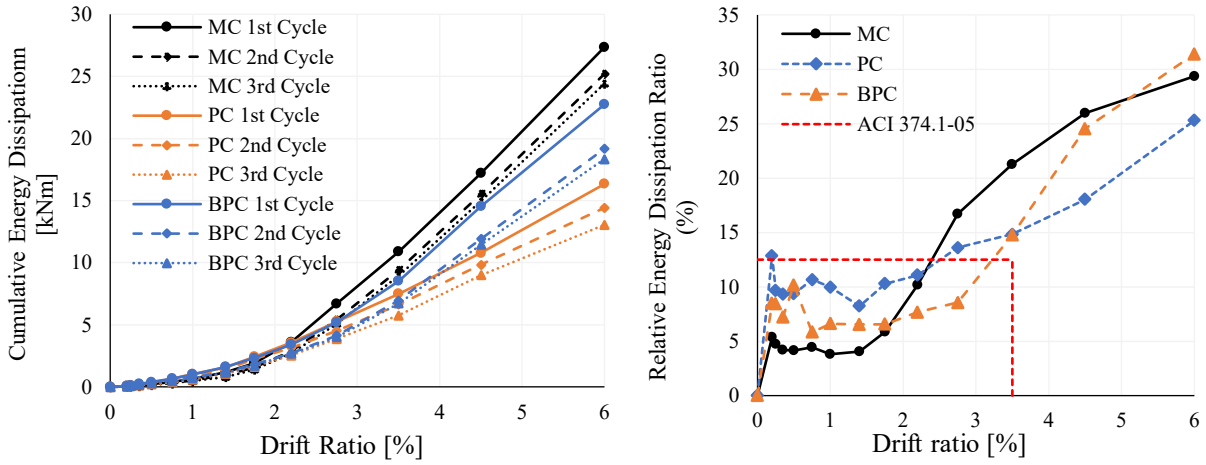

Figure 10. Energy Dissipation of Each Specimens: (a) Cumulative Energy Dissipation per Cycle; (b) Relative Energy Dissipation Ratio (REDR)

Table 6. Acceptance Criteria for Relative Energy Dissipation Ratio (REDR)

Specimen Type	REDR at the 3rd cycle, 3.5% drift (%)	Acceptance Criteria (ACI 374.1-05)
MC	21.25	Satisfied
PC	13.87	Satisfied
BPC	14.74	Satisfied

Figure 10b, supplemented by Table 6, compares the Relative Energy Dissipation Ratio (REDR) values of the three specimens along with the minimum performance threshold specified in ACI 374.1-05. The MC specimen consistently exhibited the highest REDR values beyond a *drift ratio* of 2.75%. At the reference *drift ratio* of 3.5%, as required by ACI 374.1-05, the specimen achieved a REDR of 21.25%, well above the minimum limit of 12.5%, and continued to increase to 29.36% at a *drift ratio* of 6%. In contrast, the PC specimen showed lower and relatively stable REDR values across the entire drift range. Although a slight increase was observed, the REDR reached only 13.87% at a 3.5% drift ratio, barely meeting the ACI 374.1-05 limit. This indicates that the energy dissipation capacity of the PC specimen was limited compared to that of the MC specimen. The BPC specimen demonstrated a significant upward trend in REDR after a *drift ratio* of 2.75%, even surpassing the MC specimen at 5% drift. At the reference *drift ratio* of 3.5%, the specimen recorded a REDR of 14.74%, satisfying the ACI 374.1-05 acceptance criterion. Although fluctuations occurred at lower drift levels, the sharp increase at larger drifts suggests the development of a more effective energy dissipation mechanism, likely due to anchor bar contribution and steel plate deformation. Overall, the results confirm that the MC and BPC specimens meet the REDR requirement of ACI 374.1-05 (≥12.5% at a 3.5% drift ratio), while the PC specimen only slightly exceeds this limit. The superior energy dissipation performance of MC and BPC aligns with previous findings, highlighting their greater efficiency in resisting cyclic loading compared with the PC system.

Stiffness Degradation and Displacement Ductility

Stiffness degradation refers to the reduction of a structure's ability to resist deformation under repeated loading, mainly due to microcracking and bond deterioration. This process directly decreases structural ductility. Figure 11 shows that all specimens experienced a marked stiffness reduction within the 0.5%–2.75% drift range, attributed to early structural damage — column cracking in the MC and BPC specimens, and combined column–connection damage in the PC specimen.

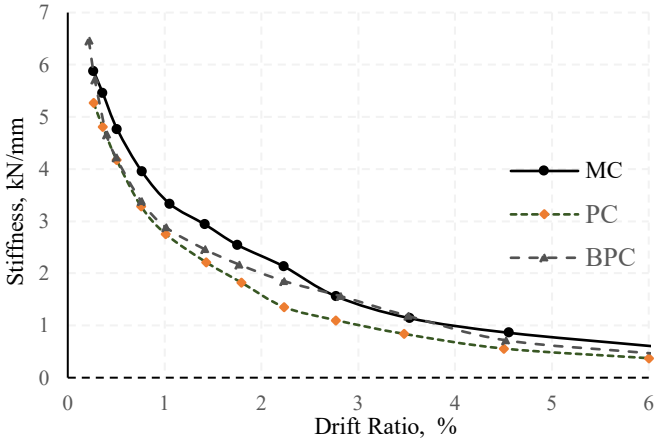

Figure 11. Stiffness Degradation

According to ACI 374.1-05, one of the acceptance criteria for moment-resisting frames concerns the secant stiffness, defined as the slope of the straight line connecting two points on the lateral force–displacement curve at ±3.5% drift during the third loading cycle. As specified in Section 9.1.3, the secant stiffness must be at least 5% of the initial stiffness obtained from the first elastic cycle. Table 7 indicates that all tested specimens satisfied this requirement, complying with the acceptance criteria of ACI 374.1-05.

Table 7. Acceptance Criteria for Secant Stiffness

Specimen	Initial Stiffness, K_0 (kN/drift)	Secant Stiffness, $K_{sec,0.35\%}^{(3)}$ (kN/drift)	Stiffness Ratio (%)	Acceptance Criteria
MC	10312.5	7131.43	69.15	Satisfied
PC	11557.62	6710	58.06	Satisfied
BPC	11342	5578.57	49.18	Satisfied

Figure 12 presents the displacement ductility analysis obtained using the Equivalent Energy Elastic–Plastic (EEEP) method in accordance with ASTM E2126-11. As summarized in Table 7, the MC specimen achieved ductility factors exceeding 9.0 in the positive direction and 9.7 in the negative direction, satisfying the requirements for a Special Moment Frame (SMF) as specified in ACI 318-19 Section 18 and ACI 374.1-05. The high ductility performance is attributed to the reinforcement detailing compliant with SMF provisions, which promotes the formation of a well defined plastic hinge mechanism and ensures efficient energy dissipation. These findings confirm that reinforcement detailing in accordance with ACI 318 SMF standards enables the development of highly deformable and seismically resilient structural behavior.

According Table 8, the PC specimen exhibited the highest ductility values, reaching 11.2 in the positive direction and over 20.7 in the negative direction. The gradual slope of the backbone curve beyond the peak load indicates that no significant column damage occurred following pocket connection failure, allowing deformation to continue without substantial loss of lateral capacity. However, despite its high ductility, the PC specimen demonstrated the lowest lateral resistance, failing to reach its probable lateral strength. Conversely, the BPC specimen exhibited lower displacement ductility compared to the MC and PC specimens, with values of 6.03 in the positive direction and 7.41 in the negative direction. Ultimate deformation occurred at drift ratios of 4.5% and 5.1%, respectively. The reduction in ductility was primarily attributed to a sharp decrease in lateral load-carrying capacity within the 3.5–4.5% drift range, caused by damage in the column base region and deformation of the steel cover plate restraining the longitudinal reinforcement. Nevertheless, the BPC specimen still achieved an average ductility greater than 6, indicating an adequate deformation capacity suitable for application in structural systems located in moderate- to high-seismic area.

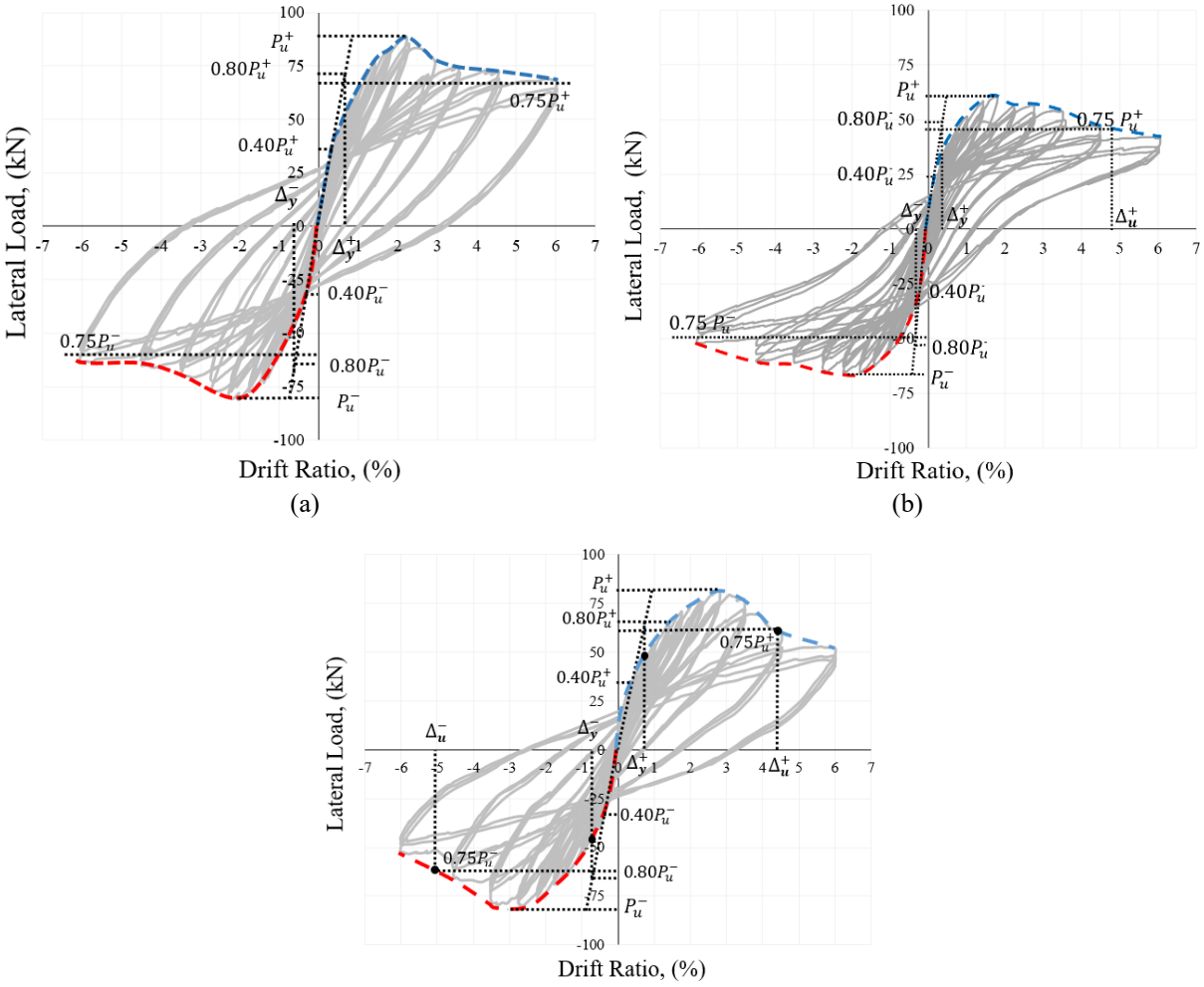

Figure 12. Displacement Ductility Curve: (a) MC; (b) PC; (c) BPC

Table 8. Comparison of Displacement Ductility Values from Each Specimen

Specimens	Cycle	P_{max}, (kN)	$P_{\Delta u}$, (kN)	$P_{\Delta y}$, (kN)	Δ_y, (mm)	Δ_u, (mm)	$\mu_\Delta = \Delta_u/\Delta_y$
MC	Positive	88.00	66.00	55.50	12.34	> 111	> 9.0
	Negative	81.00	60.75	46.50	11.47	> 111	> 9.7
PC	Positive	60.50	45.38	36.25	7.95	89.17	11.2
	Negative	66.00	49.50	33.75	5.37	> 111	> 20.7
BPC	Positive	81.50	61.13	48.00	13.51	81.40	6.03
	Negative	81.00	60.75	46.00	12.58	93.24	7.41

CONCLUSIONS

From the experimental investigation and analytical evaluation of the structural behavior of the three column–foundation connection systems (MC, PC, and BPC), the following conclusions are derived:

1. The results indicate that the connection configuration significantly influences the failure pattern and deformation capacity under cyclic loading. The MC specimen exhibited a flexural failure mechanism, with damage concentrated in the plastic hinge zone. The PC specimen failed at the connection joint before the column reached its plastic capacity. Meanwhile, the BPC specimen maintained a dominant flexural failure mechanism, despite exhibiting minor rotation at the column–foundation interface, with damage localized at the column base.
2. Based on the cyclic response, the MC specimen exhibited the highest lateral load capacity and the most stable behavior, while the PC specimen showed the lowest capacity due to grout degradation at the connection joint. The BPC specimen achieved a lateral capacity comparable to MC with more controlled damage. Overall, all specimens satisfied the nominal and maximum strength criteria specified in ACI 374.1-05, demonstrating adequate structural performance under cyclic loading.
3. Based on the energy dissipation results, the MC specimen exhibited the highest and most stable capacity, indicating good ductility and resistance to strength degradation.

4. The PC specimen showed the lowest energy dissipation due to grout failure at the connection, limiting its ability to absorb cyclic energy. The BPC specimen demonstrated improved dissipation at higher drift levels through anchor bar contribution, though slightly below the MC performance. At a 3.5% drift ratio, the REDR values of MC (21.25%) and BPC (14.74%) satisfied the ACI 374.1-05 acceptance limit (≥12.5%), while PC (13.87%) only marginally exceeded it.
5. Based on the stiffness degradation analysis, all specimens exhibited significant stiffness reduction within the 0.5%–2.75% drift range due to initial column cracking and local joint damage. Nevertheless, according to ACI 374.1-05 Section 9.1.3, all specimens satisfied the minimum secant stiffness requirement (≥5%), with stiffness ratios of 69.15% (MC), 58.06% (PC), and 49.18% (BPC), indicating adequate stiffness retention at a 3.5% drift ratio.
6. Based on the displacement ductility analysis, the MC specimen exhibited the highest ductility factor (>9.0), meeting the Special Moment Frame (SMF) requirements of ACI 318-19 and ACI 374.1-05. The PC specimen reached high numerical ductility (>20.7) due to joint rotation following grout failure, rather than genuine plastic deformation. Meanwhile, the BPC specimen showed moderate ductility (6.03–7.41), yet provided sufficient deformation capacity for structures in moderate- to high-seismic regions.

Overall, although the proposed precast connection model (BPC) did not perform as well as the monolithic system (MC), it demonstrated a balanced structural behavior characterized by a dominant flexural mechanism, good ductility, and adequate energy dissipation capacity.The BPC configuration provided a stable and controlled response under cyclic loading, indicating that it can be considered a reliable alternative for precast column–foundation connections in moderate- to high-seismic regions.

ACKNOWLEDGEMENT

This research was supported by PT. Tjakrindo Mas Concrete Division and PT. Normet Indonesia.

REFERENCES

1. Khaleghi, B., Schultz, E., Seguirant, S., Marsh, L., Haraldsson, O., Eberhard, M., and Stanton, J., Accelerated Bridge Construction in Washington State, *PCI Journal*, 55(4), 2012, pp. 34-47.
2. Ameli, M.J., Parks, J.E., Brown, D.N., and Pantelides, C.P., Seismic Evaluation of Grouted Splice Sleeve Connections for Reinforced Precast Concrete Column-to-Cap Beam Joints in Accelerated Bridge Construction, *PCI Journal,* 60(2), 2015, pp. 80-103.
3. Belleri, A. and Riva, P., Seismic Behaviour of Grouted Sleeve Precast Column-to-Foundation Connections: Results Applied to the Direct Displacement-based Design, *Proceedings of the 14th World Conference on Earthquake Engineering,* Beijing, China, October 12-17, 2008, pp. 1-8.
4. Riva, P., *Seismic Behaviour of Precast Column-to-Foundation Grouted Sleeve Connections*, Structural Engineering Department, Design and Technology Report, 2006, pp. 121-128.
5. Hofer, L., Zanini, M.A., Faleschini, F., Toska, K., and Pellegrino, C., Seismic Behavior of Precast Reinforced Concrete Column-to-Foundation Grouted Duct Connections, *Bulletin of Earthquake Engineering,* 19(12), 2021, pp. 5191-5218.
6. Yu, Z., Lv, X., Yu, Y., Ding, F., and Peng, X., Seismic Performance of Precast Concrete Columns with Improved U-Type Reinforcement Ferrule Connections, *International Journal of Concrete Structures and Materials,* 13, 2019, retrieved from https://doi.org/10.1186/s40069-019-0368-6.
7. Nascimbene, R. and Bianco, L., Cyclic Response of Column-to-Foundation Connections of Reinforced Concrete Precast Structures: Numerical and Experimental Comparisons, *Engineering Structures,* 247, 2021, 113214.
8. Cogurcu, M.T. and Uzun, M., Experimental Investigation of a New Precast Column-Foundation Connection under Cyclic Loading, *Journal of Building Engineering,* 50, 2022, 104245.
9. Su, H., Yang, C., Fan, W., Sun, C., and Guo, W., Hysteresis Characteristics of Multi-Segment Precast Columns with Ultra-High-Performance Concrete-based Grouted Sleeve Connections: An Experimental and Analytical Approach, *Engineering Structures*, 322, 2025, 119157.
10. Liu, H., Yan, Q., and Du, X., Seismic Performance Comparison between Precast Beam Joints and Cast-In-Place Beam Joints, *Structural Concrete,* 17(1), 2016, pp. 100-111.
11. Camnasio, E. and Kiriakopoulos, P., Investigation on Bolted Precast Column Connection for Seismic Applications, *Proceedings of the 16th European Conference on Earthquake Engineering (16ECEE),* Thessaloniki, Greece, June 18-21, 2018, pp. 1-8.
12. Metelli, G., Beschi, C., and Riva, P., Cyclic Behaviour of a Column-to-Foundation Joint for Concrete Precast

Structures, *European Journal of Environmental and Civil Engineering,* 15(9), 2011, pp. 1297-1318.
13. Ye, C., Ruan, R., Luo, Y., Zhang, R., and Zeng, Z., Experimental and Numerical Investigation on Seismic Performance of Bolted Connection Precast Concrete Column-Footing Joints, *Structures,* 80, 2025, 109901.
14. Ben Gu, J., Wang, Y.F., Tao, Y., Yuan, S.L., and Deng, X.M., Seismic Performance of Precast Reinforced Concrete Columns Employing UHPC Connections, *Structures,* 80, 2025, 109969.
15. Li, J., Wang, W., Chen, P., Chen, J., and Ma, J., Post-fire Seismic Performance of Precast Concrete Columns with Grouted Sleeve Connections: An Experimental Study, *Structures,* 66, 2024, 106816.
16. Dal Lago, B., Toniolo, G., and Lamperti Tornaghi, M., Influence of Different Mechanical Column-Foundation Connection Devices on the Seismic Behaviour of Precast Structures, *Bulletin of Earthquake Engineering,* 14(12), 2016, pp. 3485-3508.
17. Fan, J.J., Feng, D.C., Wu, G., Hou, S., and Lu, Y., Experimental Study of Prefabricated RC Column-Foundation Assemblies with Two Different Connection Methods using Large-Diameter Reinforcing Bars, *Engineering Structures,* 205, 2020, 110075.
18. Zhou, X., Ding, R., Guo, B., Nie, X., and Fan, J., Connections between Precast Hollow Concrete Columns and Foundations using UHPC and Rebar Lap Splices, *Engineering Structures, 321,* 2024, 118982.
19. Aboukifa, M.A., Reyad, K.H., and Saad, F.A., Behavior and Design of Precast Column/Base Pocket Connections with Smooth Surface Interface, *HBRC Journal,* 13(1), 2017, pp. 39-49.
20. Pereiro-Barceló, J., Bonet, J.L., Rueda-García, L., and Albiol-Ibáñez, J.R., Cyclic Response of Precast Column-to-Foundation Connection using UHPC and Ni-Ti SMA Reinforcements, *Engineering Structures,* 252, 2022, 113624.
21. Hemamathi, L. and Jaya, K.P., Behaviour of Precast Column-Foundation Connection under Reverse Cyclic Loading, *Advances in Civil Engineering,* 2021, Article ID 6677007, 17 pages, retrieved from https://doi.org/10.1155/2021/6677007.
22. Zhang, G., Han, Q., Xu, K., Du, X., and He, W., Quasi-static Tests of CFST Embedded RC Column-to-Precast Cap Beam with Socket Connection, *Engineering Structures,* 241, 2021, 112443.
23. Ma, H., Lai, M., Shi, X., Cao, Z., and Zhou, J., Experimental and Numerical Study on Column-Foundation Connection through External Socket, *Journal of Civil Engineering and Management,* 27(3), 2021, pp. 162-174.
24. Constantinescu, H. and Toader, T.-N., Structural Design and Technology of Pocket Foundations for Long Precast Concrete Columns in Seismic Areas, *Buildings*, 14(11), 2024, 3466, retrieved from https://doi.org/10.3390/buildings14113466.
25. Golewski, G.L., The Specificity of Shaping and Execution of Monolithic Pocket Foundations (PF) in Hall Buildings, *Buildings,* 12(2), 2022, 192, retrieved from https://doi.org/10.3390/buildings12020192.
26. Haraldsson, O.S., Janes, T.M., Eberhard, M.O., and Stanton, J.F., Seismic Resistance of Socket Connection between Footing and Precast Column, *Journal of Bridge Engineering,* 18(9), 2013, pp. 910-919.
27. Canha, R.M.F., Jaguaribe, K.B., El Debs, A.L.H.C., and El Debs, M.K., Analysis of the Behavior of Transverse Walls of Socket Base Connections, *Engineering Structures,* 31(3), 2009, pp. 788-798.